FACTA UNIVERSITATIS
Series: **Physics, Chemistry and Technology** Vol. 18, Nº 2, 2020, pp. 119 - 129
https://doi.org/10.2298/FUPCT2002119A

STRUCTURAL, MAGNETIC AND UP-CONVERSION PROPERTIES OF YF_3: Yb/*Ln* (*Ln* = Er, Tm, Ho) SOLID SOLUTIONS†

UDC 546.650 + 661.866.8

Jelena Aleksić[1], Tanja Barudžija[2], Miodrag Mitrić[2], Marko Bošković[2], Zoran Ristić[2], Ljiljana Kostić[1]

[1]University of Niš, Faculty of Sciences and Mathematics, Department of Physics, Niš, Serbia
[2] Vinča Institute of Nuclear Sciences – National Institute of the Republic of Serbia, University of Belgrade, P.O. Box 522, Belgrade, Serbia

Abstract. *In this paper, we investigated YF_3: Yb/Er, YF_3: Yb/Tm, and YF_3: Yb/Ho solid solutions prepared by reaction of an appropriate amount of oxides with ammonium difluoride (NH_4HF_2) as a fluorinating agent. These samples were characterized by X-ray diffraction (XRD), magnetic measurements, and up-conversion (UC) photoluminescence spectra. The results show that all samples are single-phase and crystallize in an orthorhombic crystal structure of the β-YF_3 structure type. Above 100 K, the measured molar magnetic susceptibility was fitted by the Curie-Weiss law and the average effective magnetic moments for the observed samples were obtained. All the samples showed pure paramagnetic behavior. When doped with lanthanide elements (Yb/Er, Yb/Tm, Yb/Ho), YF_3 solid solutions can emit characteristic green, red, blue, and near IR light under the excitation of a 980 nm laser diode.*

Key words: *lanthanides, up-conversion, X-ray diffraction, magnetic measurements*

1. INTRODUCTION

In the last decades, lanthanide-doped up-conversion (UC) nanomaterials have attracted a lot of attention in the fields such as solid-state lasers, solar cells, temperature sensors, medical diagnostics, biomarkers, fiber-optic communication systems, ratiometric thermometry, etc. (Atabaev, 2019, Dramićanin, 2018, Escudero et al., 2017, Ho et al., 2019, Liu et al., 2011, Tiwari, 2018). These materials owe their popularity to their specific

Received November 29th, 2020; accepted December 27th, 2020
†Acknowledgement: The authors thank the support by the Ministry of Education, Science and Technological Development of the Republic of Serbia under Contract No. 451-03-68/2020-14/200124.
* **Corresponding author**: Jelena Aleksić, Department of Physics, Faculty of Sciences and Mathematics, University of Niš, Višegradska 33, 18000 Niš, Serbia
E-mail: jelena.aleksic@pmf.edu.rs

© 2020 by University of Niš, Serbia | Creative Commons License: CC BY-NC-ND

ability to convert near-infrared to high-energy photons (visible or ultraviolet), a process that results from the abundance of energy levels of 4f configurations (Atabaev, 2019, Auzel, 2003). They also possess significant chemical stability and photostability, multicolor emission, and great anti-Stokes shift. When it comes to biological applications, these materials reduce photodamage and enable high penetration of light into tissues, and, most importantly, they have a small level of toxicity (Duan et al., 2018, Zhao et al., 2020, Zhu et al, 2018).

Among many possible UC matrices, such as fluorides, oxides, vanadates, and phosphates, the first ones have attracted the most attention in research to date. The YF_3 matrix is a very suitable host due to its chemical and thermal stability, high refractive index, and possession of optical transparency in a wide range of wavelengths (Wang et al., 2010). Its low maximum phonon energy (about 400 cm^{-1}) reduces the non-radiative quenching of excited sites of lanthanide (*Ln*) ions to the minimum. The similar radii of Y^{3+} ions to other Ln^{3+} ions enable the easy embedding of Ln^{3+} ions in a YF_3 host matrix into the Y^{3+} sites (Shannon and Prewitt, 1970).

As this topic is attractive, there are many methods of synthesis used (perhaps solvothermal and hydrothermal synthesis are the most frequent) to obtain samples of uniform dimension and regular morphology (Han et al., 2014, He et al., 2014, Xiang et al., 2015). In this, similar to our previous works (Aleksić et al., 2020, Ćirić et al., 2020), we use the method of fluorination of appropriate oxides with ammonium hydrogen difluoride (NH_4HF_2). This method is one of the most convenient for getting oxygen-free fluorides, as it is simple and does not need some complicated and expensive equipment for realization.

Doping YF_3 with different lanthanides leads to obtaining materials that can emit light of different colors such as green, red, blue, near UV and near-infrared, under the 980 nm laser excitation (De et al., 2007, Ding et al., 2013, Li et al., 2017, Tang et al., 2018). The laser diode producing 980 nm light is an attractive and powerful excitation source, in contrast to its relatively low price. With this light source, the Yb^{3+} ion often acts as a sensitizer due to its high absorption cross-section at 980 nm wavelength. Moreover, this wavelength is characterized by the maximum penetration depth into biological tissues. Er^{3+}, Tm^{3+}, and Ho^{3+}, probably the most used lanthanide ions for luminescent measurements, serve as activators, with their emissions primarily being fuelled by energy transferred from Yb^{3+} ions in their excited states.

In our research, we observed the structural, optical, and magnetic behavior of YF_3 doped with the following pairs of lanthanide ions Yb^{3+}/Er^{3+}, Yb^{3+}/Tm^{3+}, Yb^{3+}/Ho^{3+}.

2. EXPERIMENTS

All investigated YF_3: Yb/Er; YF_3: Yb/Tm; YF_3: Yb/Ho solid solutions were prepared by mixing the appropriate amount of required oxides with ammonium hydrogen difluoride. All chemicals used in the reactions were acquired from Sigma−Aldrich and are of 98.5–99.99 % purity. The final samples were obtained in two steps. First, the grounded homogenous mixture was heated at 170 °C for 20 hours in the air and then was heated further for 3 hours at 500 °C in a reducing atmosphere (Ar-10% H_2). The overall reaction of synthesizing $Y_{0.78}Yb_{0.2}Ln_{0.02}F_3$ (with *Ln* = Er, Tm, Ho) is given by the following:

$$0.78Y_2O_3 + 0.2Yb_2O_3 + 0.02Ln_2O_3 + 6NH_4HF_2 \rightarrow$$
$$2Y_{0.78}Yb_{0.2}Ln_{0.02}F_3 + 6NH_4F + 3H_2O. \quad (1)$$

X-ray diffraction (XRD) measurements of the synthesized samples were examined on a Philips PW 1050 diffractometer with Cu Kα radiation (λ = 1.54178 Å). X-ray measurements were done within the 2θ range of 10° to 120°, with a step of 0.02° and a counting time of 12 s. We refined the structure of all samples using Rietveld full profile analysis (Rietveld, 1969). This analysis was performed in the FullProf program packet (Rodriguez-Carvajal, 1993) using the Thompson-Cox-Hastings pseudo-Voight function. For treating the crystallite size of samples, we used the spherical harmonic model, whereas for the microstrain on peak broadening, we utilized the quadratic form model in reciprocal space.

Photoluminescence measurements of all three prepared samples were acquired on a Fluorolog-3 spectrofluorometer (model FL3–221, Horiba Jobin Yvon, emission slit set to 1 nm). For the excitation, a solid-state 980 nm laser (model MDLH 980 3 W, the excitation power set to 150 nW) was used. For photoluminescence measurements, powder samples were pressed under the load of 2000 kg/cm^2 to obtain pellets.

The magnetic behavior of prepared samples was observed by MPMS SQUID magnetometer from Quantum Design.

3. Results and Discussion

3.1. XRD analysis

We have checked the phase purity and the crystal structure of the synthesized powders by XRD measurements (Figure 1). According to the phase analysis, all samples are single-phase and crystalize in the β-YF_3 type orthorhombic crystal structure (S.G. Pnma, No. 62). Hence, we could say that Yb^{3+} and Ln^{3+} ions (*Ln* = Er, Tm, Ho) are fully incorporated into the YF_3 host matrix replacing the Y^{3+} sites. In this type of crystal structure, cations occupy the 4*c* Wyckoff position (*x*, ¼, *z*) whereas the fluorine ions occupy the 4*c* (*x*, ¼, *z*) and 8*d* general position (*x*, *y*, *z*).

The structure parameters of our samples were refined using the starting parameters from Ref. (Zalkin and Templeton, 1953). Some most important parameters from Rietveld analysis (lattice constants, cell volume, profile R-factors, crystallite size, microstrain) are summarised in Table 1. There is a noticeable slight decrease in lattice constants in comparison to the starting data from (Zalkin and Templeton, 1953). This is the consequence of the different ionic radii of Y^{3+} ions and the ions of the selected lanthanides (Yb^{3+}, Er^{3+}, Tm^{3+}, Ho^{3+}) which are built in the YF_3 matrix (Shannon and Prewitt, 1970). The effective radii of ions incorporated in the host matrix are smaller than the effective radii of Y^{3+} ions. In descending order, their radii r are given by: $r(Y^{3+}) > r(Ho^{3+}) > r(Er^{3+}) > r(Tm^{3+}) > r(Yb^{3+})$. The average crystallite size of all solid solutions is about 50 nm, with the average maximum microstrain of about 0.2%. Figure 2 presents the final Rietveld plots for YF_3: Yb/Er; YF_3: Yb/Tm; YF_3: Yb/Ho samples.

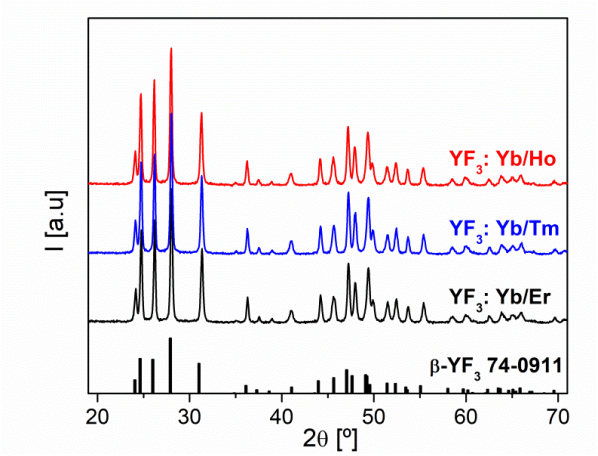

Fig.1 XRD patterns of final samples.

3.2. Magnetic measurements

Figure 3 shows the temperature dependence of the inverse susceptibilities for all three synthesized samples. The experimental data were corrected by subtracting the diamagnetic contribution using values given in Bain and Berry (2008). As we can notice from Figure 3, the dependence of the inverse susceptibility upon the temperature does not follow the Curie-Weiss law in the whole temperature range. This is a consequence of the crystal field acting on the lanthanide ions. Since the ions are built into a host, the energy levels of the lanthanide ions become affected by the crystal field of the host material and split into several Stark levels (Qiu et al., 2013). This splitting caused by the crystal field is incomparably smaller (~ few hundred cm^{-1}) than the energy distance of different multiplets. The number of Stark levels of the exact level in question depends on the total orbital quantum number J of that level, the number of electrons of the exact lanthanide ion, as well as the symmetry and intensity of the external crystal field. According to Kramer's theorem, the maximum number of Stark levels into which the energy level splits depends on the number of electrons, more precisely whether that number is odd or even. If the number of electrons of lanthanide ions is odd, the energy level can be split into a maximum of $(2J+1)/2$ Stark levels, whereas if the number is even, the maximum number of Stark levels is $2J+1$. As mentioned previously, the number of Stark levels also depends on the crystal field symmetry. In the problem at hand, lanthanide ions are embedded in the yttrium position 4c, with C_s symmetry. Located in the crystal field with symmetry lower than cubic, Yb^{3+} ($^2F_{7/2}$) and Er^{3+} ($^4I_{15/2}$), ground terms split into four and eight Kramer's doublets, respectively. In contrast to this, non-Kramer's ions, such as Tm^{3+} and Ho^{3+} can have singlet and doublet Stark levels, depending on symmetry positions.

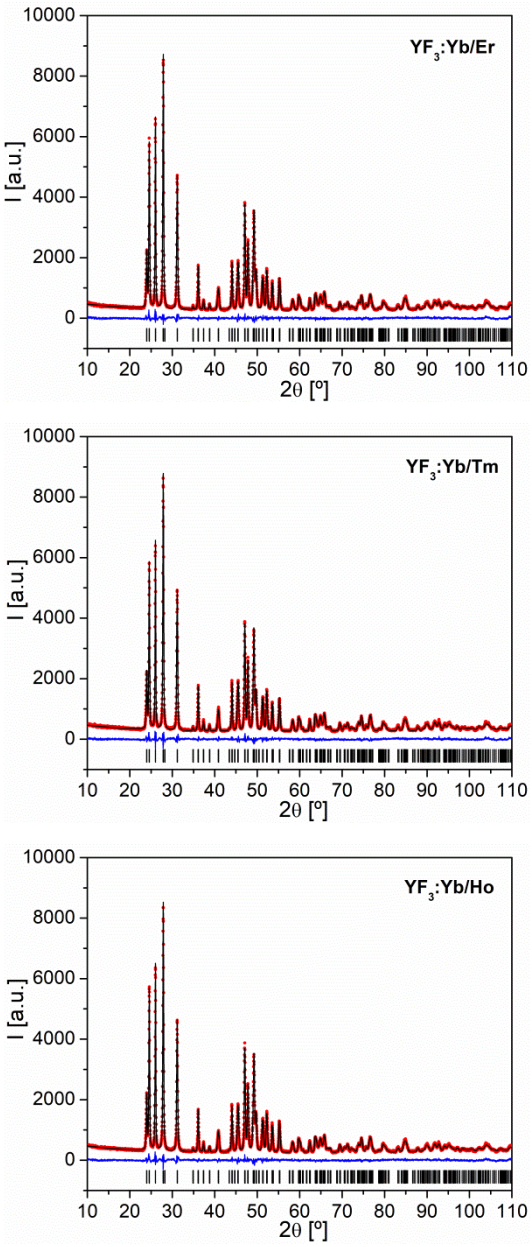

Fig. 2 The final Rietveld plots for YF_3: Yb/Er, YF_3: Yb/Tm, and YF_3: Yb/Ho samples. Red circles represent observed intensities, the black line represents the calculated intensities, and the solid blue line represents the difference in observed and calculated intensities. The vertical black bars indicate the positions of Bragg peaks.

Table 1 The main results of the structure refinement of YF_3: Yb/*Ln* (*Ln* = Er, Tm, Ho).

Samples		$Y_{0.78}Yb_{0.2}Er_{0.02}F_3$	$Y_{0.78}Yb_{0.2}Tm_{0.02}F_3$	$Y_{0.78}Yb_{0.2}Ho_{0.02}F_3$
a(A)		6.32113 (10)	6.32252 (10)	6.32273 (10)
b(A)		6.84292 (12)	6.84385 (11)	6.84381 (12)
c(A)		4.41623 (7)	4.41580 (7)	4.41622 (7)
Cell volume, V (A^3)		191.024 (5)	191.073 (5)	191.097 (5)
Profile R-factors:				
R_{wp}		8.34 %	8.64 %	8.36 %
R_{exp}		8.17 %	8.23 %	8.25 %
Bragg R-factor, R_B		3.062 %	3.333 %	3.136 %
Chi^2		1.054	1.10	1.03
Y, Yb, *Ln* ($4c$)	x	0.36786 (8)	0.36791 (8)	0.36786 (8)
	z	0.05708 (10)	0.05721 (11)	0.05707 (10)
	B_{iso} (A^2)	2.13 (2)	2.12 (2)	2.16 (2)
F ($4c$)	x	0.5235 (4)	0.5234 (4)	0.5234 (4)
	z	0.5939 (6)	0.5950 (7)	0.5946 (6)
	B_{iso} (A^2)	1.93 (7)	1.87 (7)	1.92 (7)
F ($8d$)	x	0.1647 (4)	0.1649 (4)	0.1648 (4)
	y	0.0621 (2)	0.0624 (2)	0.0622 (2)
	z	0.3712 (4)	0.3706 (4)	0.3711 (4)
	B_{iso} (A^2)	2.17 (6)	2.10 (6)	2.14 (5)
Average crystallite size (nm)		50	51	49
Average maximum microstrain (%)		0.23	0.20	0.22

In the high-temperature range, the measured molar magnetic susceptibility for all three samples can be fitted by the Curie-Weiss law:

$$\chi^{-1} = \frac{T-\theta}{C}, \tag{2}$$

where C is the Curie constant and θ is the Curie-Weiss temperature. The values of C and θ are determined from the fit in the 100–300 K region, and the obtained values for all three compounds are presented in Table 2. The obtained value of the Curie constant was used for the calculation of the average effective magnetic moment (Antić et al., 1995):

$$\mu_{eff}^{exp} \approx \sqrt{8C}\mu_B, \tag{3}$$

where μ_B denotes the Bohr magneton. The effective magnetic moments determined from the fits are $2.486\mu_B$, $2.367\mu_B$, and $2.524\mu_B$ for YF_3: Yb/Er, YF_3: Yb/Tm, and YF_3: Yb/Ho samples, respectively. The effective magnetic moments of these samples can be calculated via the following equation (Hirose et al., 2009):

$$[\mu_{eff}^{cal}]^2 = 0.2[\mu_{eff}]_{Yb^{3+}}^2 + 0.02[\mu_{eff}]_{Ln^{3+}}^2 \tag{4}$$

where $[\mu_{eff}]_{Yb^{3+}}$ and $[\mu_{eff}]_{Ln^{3+}}$ are the free ion magnetic moments of Yb^{3+} and Ln^{3+} ions. From Table 2, we can conclude that the effective moments obtained by the experiment are consistent with the moments calculated using the equation (3). Negative values of the Curie-Weiss temperature θ show the predominant antiferromagnetic interactions between the lanthanide ions.

The field dependence of the isothermal magnetization, measured at the temperature of 2K, is presented in Figure 4. The absence of hysteresis shows a pure paramagnetic behavior of our prepared samples. These $M(H)$ curves can be fitted by the Langevin function (Blundell, 2001):

$$M = M_s L(y) = M_s \left[\coth y - \frac{1}{y}\right], \tag{5}$$

where M_s is the magnetization obtained when all the magnetic moments are aligned, $y = \mu B/k_B T$, μ is the magnetic moment of the ion, B is the magnetic field and k_B is the Boltzmann's constant. Since the Langevin function neatly fits the experimental data $M(H)$, the pure paramagnetic behavior of all synthesized samples is confirmed.

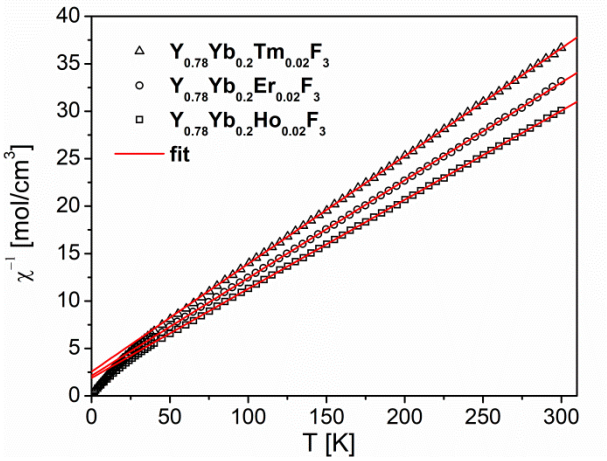

Fig. 3 The inverse susceptibilities χ^{-1}(T) for YF_3: Yb/Er, YF_3: Yb/Tm, and YF_3: Yb/Ho samples (open symbols) fitted to the Curie-Weiss law in the temperature range 100–300 K (solid lines).

Table 2 Curie-Weiss temperatures, Curie constants, and the effective magnetic moments (μ_{eff}^{exp}: experimental, μ_{eff}^{cal}: calculated) for YF_3: Yb/Ln.

Ln	$\boldsymbol{\theta}$	$\boldsymbol{C}$ ($\frac{\text{emu K}}{\text{mol Oe}}$)	$\boldsymbol{\mu_{eff}^{exp}(\mu_B)}$	$\boldsymbol{\mu_{eff}^{cal}(\mu_B)}$
Er	-20.6(3)	0.772(1)	2.486(5)	2.442
Tm	-22.5(2)	0.7004(7)	2.367(3)	2.295
Ho	-20.1(2)	0.8469(8)	2.524(4)	2.603

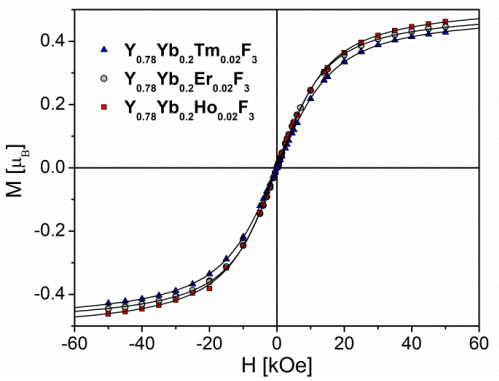

Fig. 4 The isothermal magnetization $M(H)$ for YF_3: Yb/Er, YF_3: Yb/Tm, and YF_3: Yb/Ho samples at 2 K. The full lines represent the calculated curves.

3.3. Upconversion spectra of YF_3: Yb/Er; YF3: Yb/Tm and YF_3: Yb/Ho

The upconversion (UC) emission spectra of the prepared YF_3:Yb/Ln^{3+} (with *Ln* = Er, Tm, Ho) samples that occurred under the excitation of the laser source of 980 nm are presented in Figure 5. These UC spectra are recorded in the range of 350–700 nm for samples doped with Er^{3+} ions, and in the range of 250–920 nm for Tm^{3+} and Ho^{3+} doped samples. In the UC spectrum of YF_3:Yb^{3+}/Tm^{3+} (Figure 5a), we notice three emission bands located at 477 nm, 700 nm, and 807 nm, that originate from ${}^1G_4 \rightarrow {}^3H_6$, ${}^3F_{2,3} \rightarrow {}^3H_6$ and ${}^3H_4 \rightarrow {}^3H_6$ transitions of Tm^{3+}, respectively. The most intensive band in this spectrum is the near-infrared emission centered at 807 nm. For the YF_3:Yb^{3+}/Ho^{3+} sample, emission bands are centered at 543 nm, 650 nm, and 748 nm, and can be matched with ${}^5S_2/{}^5F_4 \rightarrow {}^5I_8$, ${}^5F_5 \rightarrow {}^5I_8$ and ${}^5S_2/{}^5F_4 \rightarrow {}^5I_7$ transitions of the Ho^{3+}, respectively. In this UC spectrum, the most intensive is the green emission associated with the ${}^5S_2/{}^5F_4 \rightarrow {}^5I_8$ transition. In the third spectrum that is associated with YF_3:Yb^{3+}/Er^{3+}, we can recognize three emission bands centered at 524 nm, 542 nm, and 660 nm. These bands correspond to ${}^2H_{11/2} \rightarrow {}^4I_{15/2}$, ${}^4S_{3/2} \rightarrow {}^4I_{15/2}$ and ${}^4F_{9/2} \rightarrow {}^4I_{15/2}$ transitions, respectively. There is the complete domination of the green band (transition ${}^4S_{3/2} \rightarrow {}^4I_{15/2}$) over the red band (transition ${}^4F_{9/2} \rightarrow {}^4I_{15/2}$), which is in contrast with Ref. (Xiang et al., 2015).

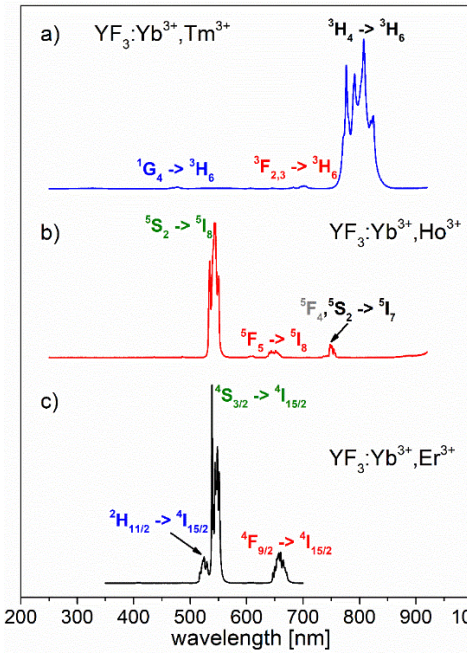

Fig. 5 UC spectra from (a) YF_3:Yb/Tm; (b) YF_3:Yb/Ho, and (c) YF_3:Yb/Er.

If we look at the most dominant transitions of all prepared samples, we can notice that subcomponents of these bands, which occurred by the action of the crystal field, are spectrally well resolved. This confirms the good crystallinity of our samples. The ratio of the emission bands and the number of UC emission occurred in the spectra could vary depending on the concentration of lanthanide ions, the method of preparation of the samples, sample size, shape, and presented defects (Payrer et al., 2017, Tang et al., 2018, Weng et al., 2009). The scheme of the population of high-energy levels in the Er^{3+}, Ho^{3+}, Tm^{3+} ions occurs through a well-known mechanism.

Since lanthanide ions, such as Er^{3+}, $Ho^{3+,}$ and Tm^{3+}, do not have energy levels resonant with 980 nm, the Yb^{3+} ions, which have a high absorption coefficient in the range of the laser pump, absorb the pump light and transit from the ground state ($^2F_{7/2}$) to the first excited state ($^2F_{5/2}$). Excited Yb^{3+} ions serve as sensitizers and transfer energy to the surrounding acceptor ions, such as Er^{3+}, Tm^{3+}, and Ho^{3+}, thereby exciting the ions to the $^4I_{11/2}$, $^3H_5$ and $^5I_6$ states, respectively. Excited acceptor ions can relax to the lower energy levels or can receive extra energy from two or more donors and to be excited into the higher levels. Afterward, the ions can relax to the ground state or interstates via UC emissions. If two or more Yb^{3+} ions transfer energy to the same acceptor ion, this ion can emit luminescence in the near IR or visible wavelengths. The proposed UC scheme that occurs in our samples is presented in Figure 6.

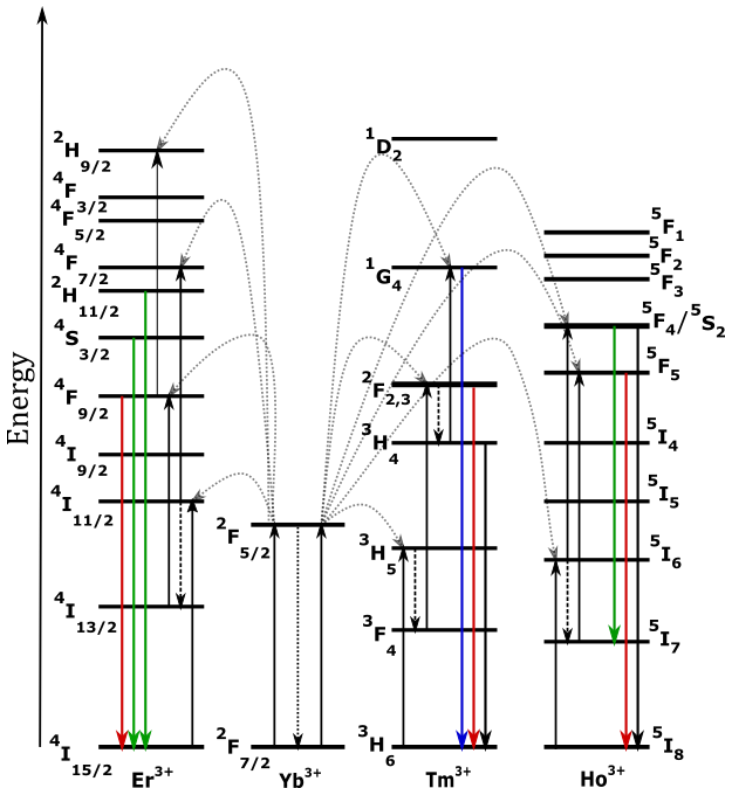

Fig. 6 The suggested UC energy transfer mechanism of the YF_3:Yb^{3+}/Tm^{3+}, YF_3:Yb^{3+}/Ho^{3+} and YF_3:Yb^{3+}/Er^{3+} samples occurred under the excitation of the laser source of 980 nm.

4. CONCLUSION

The polycrystalline YF_3: Yb/*Ln* (*Ln* = Er, Tm, Ho) samples were synthesized by the fluorination of a mixture of the appropriate oxide with ammonium hydrogen difluoride. All obtained samples are of good crystallinity and crystalize in the orthorhombic crystal structure of the β-YF_3 type. The temperature dependence of the inverse susceptibilities mismatches the Curie-Weiss law in the whole temperature range for all three samples, which is a consequence of the action of the crystal field on the lanthanide ions. In contrast to this, in the high-temperature range (above 100 K), magnetic susceptibility can be fitted by the Curie-Weiss law. The values of the average effective magnetic moments, determined from the fitting parameter *C*, are $2.486\mu_B$, $2.367\mu_B$, and $2.524\mu_B$ for YF_3: Yb/Er, YF_3: Yb/Tm, and YF_3: Yb/Ho samples, respectively. These values are in agreement with the values calculated using the effective magnetic moments of free lanthanide ions. The obtained fitting parameters for the Curie-Weiss temperature θ are all negative, which indicates the predominant antiferromagnetic interaction between the lanthanide ions. The field dependence of the isothermal magnetization can be fitted by the Langevin function, which confirms the pure paramagnetic behavior of all synthesized solid solutions. The up-conversion spectra show that the prepared solid solutions can emit characteristic blue, red, green, and near IR light under a 980 nm laser excitation. In the YF_3: Yb/Tm sample, the most intensive is the near-infrared line located at 807 nm, while with YF_3: Yb/Er and YF_3: Yb/Ho the most intensive are the green lines located at 542 nm and 543 nm, respectively.

REFERENCES

Aleksić, J., Barudžija, T., Jugović, D., Mitrić, M., Bošković, M., Jagličić, Z., Lisjak, D. and Kostić, Lj., 2020, J. Phys. Chem. Solids, 142, 109449. doi:10.1016/j.jpcs.2020.109449
Antić B., Mitrić M., Rodić, D., 1995, J. Magn. Magn. Mater., 145, 349-356. doi:10.1016/0304-8853(94)01625-9
Atabaev, TS., Molkenova, A., 2019, Front. Mater. Sci., 13, 335-341. doi:10.1007/s11706-019-0482-z
Auzel, F., 2003, Chem. Rev., 104, 139-174. doi:10.1021/cr020357g
Bain, G., Berry, J., 2008, J. Chem. Educ., 85, 1-5. doi:10.1021/ed085p532
Blundell, S., 2001, Magnetism in Condensed Matter, Oxford University, New York
Ćirić, A., Aleksić, J., Barudžija, T., Antić, Ž., Đorđević, V,. Medić, M., Periša, J., Zeković, I., Mitrić, M., Dramićanin., M., 2020, Nanomaterials, 10, 1-10. doi:10.3390/nano10040627
De, G., Qin, W., Zhang, J., Zhang, J., Wang, Y., Cao, C., Cui Y., 2007, J. Lumin., 122-123, 128-130. doi:10.1016/j.jlumin.2006.01.120
Ding, M., Lu, C., Cao, L., Ni, Y., Xu, Z., 2013, Funct. Mater. Lett, 6, 1350061. doi:10.1142/S1793604713500616
Dramićanin, M., 2018, Luminescence Thermometry, 1st ed. Woodhead Publishing, UK.
Duan, C., Liang, Li. And Li. L, 2017, J. Mater. Chem. B, 6, 192-209. doi:10.1039/C7TB02527K
Escudero, A., Becerro, A., Carrion, C., Nunez, N., Zyuzin, M., Laguna, M., Gonzales-Mancebo. D., Ocana, M., Parak, W., 2017, Nanophotonics, 6, 881-921. doi:10.1515/nanoph-2017-0007
Han, L., Wang, Y., Guo, L., Zhao, L., Tao, Y., 2014, Nanoscale, 6, 5907-5917. doi:10.1039/C4NR00512K
He, F., Wang, L., Niu, N., Ga, S., Wang, Y., Yang, P., 2014, J. Nanosci. Nanotechnol., 14, 3503-3508. doi:10.1166/jnn.2014.7975
Hirose, K., Doi, Y., Hinatsu, Y., 2009, J. Solid State Chem., 182, 1624-1630. doi:10.1016/j.jssc.2009.04.001
Ho, WJ., Wei, CY., Liu, Jj., Lin, WC., Ho, CH., 2019, Vacuum, 166, 1-5. doi:10.1016/j.vacuum.2019.04.046
Li, H., Huang, Q., Wang, Y., Chen, K., Xie, J., Pan, Y., Su, H., Xie, X., Huang, L., Huang, W., 2017, J. Mater. Chem. C, 5, 6450-6456. doi:10.1039/C7TC02118F
Liu, TC., Cheng, BM., Hu, SF., Liu. RS., 2011, Chem. Mater., 23, 3698-3705. doi:10.1021/cm201289s
Payrer, E. L., Joudrier, A. L., Aschehoug, P., Almeida, RM., Deschanvres, JL., 2017, J. Lumin, 187, 247-254. doi:10.1016/j.jlumin.2017.02.051
Rietveld, HM., 1969, J. Appl. Crystallogr, 2, 65-71. doi:10.1107/S0021889869006558
Rodriguez-Carvajal J., 1993, Physica B, 192, 55-69.

Shannon, RD., Perwitt, CT., 1970, Acta Cryst. B, 26, 1046-1048. doi:10.1107/S0567740870003576
Steinkemper, H., Fisher, S., Hermle, M., Goldschmidt JC., 2013, New J. Phys., 15. doi:10.1088/1367-2630/15/5/053033
Tang, J., Yu, M., Wang, E., Ge, C., Chen, Z., 2018, Mater. Chem. Phys., 207, 530-533. doi:10.1016/j.matchemphys.2018.01.017
Tiwari, S., Maurya, S., Yadav, R., Kumar, A., Kumar, V., Joubert, MF., Swart, H., 2018, J. Vac. Sci. Technol., 36. doi:10.1116/1.5044596
Wang, S., Song, S., Deng, R., Guo, H., Lei, Y., Cao, F., Li, X., Su, S., Zhang, H., 2010, CrysEngComm, 12, 3537-3541. doi:10.1039/C0CE00023J
Weng, F., Chen, D., Wang, Y., Yu, Y., Huang, P., Lin, H., 2009, Ceram. Int., 35, 2619-2623. doi:10.1016/j.ceramint.2009.02.026
Xiang, G., Zhang, J., Hao, Z., Pan, GH., Chen, L., Luo, Y., Lu, S., Zhao, H., 2015, J. Colloid Interface Sci., 459, 224-229. doi:10.1016/j.jcis.2015.08.026
Zalkin, A., Templeton, DH., 1953, J. Am. Chem. Soc., 75, 2453-2458, doi:10.1021/ja01106a052
Zhao, Y., Wang, X., Zhang, Y., Li, Y., Yao, X., 2020, J. Alloys Compd., 817, 152691. doi:10.1016/j.jallcom.2019.152691
Zhu, X., Li, J., Qiu, X., Liu, Y., Feng, W., Li, F., 2018, Nat. Commun., 9. doi:10.1038/s41467-018-04571-4

STRUKTURNE, MAGNETNE I UP-KONVERZIONE OSOBINE ČVRSTIH RASTVORA YF_3: Yb/*Ln* (*Ln* = Er, Tm, Ho)

U radu su vršena ispitivanja čvrstih rastvora YF_3: Yb/Er, YF_3: Yb/Tm i YF_3: Yb/Ho, pripremljenih hemijskom reakcijom između odgovarajućih količina oksida retkih zemalja i amonijum-bifluorida (NH_4HF_2). Dobijeni uzorci su ispitivani korišćenjem rendgenske analize, magnetnih i luminescentnih merenja. Rezultati pokazuju da su sva jedinjenja jednofazna i da kristališu sa ortorombičnom β-YF_3 kristalnom strukturom. Na temperaturama iznad 100 K, izmerena molarna magnetna suseptibilnost je fitovana Kiri-Vajsovim zakonom i izračunati su srednji efektivni magnetni momenti posmatranih uzoraka. Svi uzorci su pokazali čisto paramagnetno ponašanje. Čvrsti rastvori YF_3, dopirani lantanidima (Yb/Er, Yb/Tm, Yb/Ho), usled ekscitacije laserskom diodom talasne dužine 980 nm, mogu emitovati karakteristično zeleno, crveno, plavo i blisko infracrveno svetlo.

Ključne reči: *lantanidi, up-konverzija, difrakcija X-zraka, magnetna merenja*